nature communications

Article

https://doi.org/10.1038/s41467-025-59990-x

On-demand tailoring soliton patterns through intracavity spectral phase programming

Received: 22 October 2024

Accepted: 9 May 2025

Published online: 21 May 2025

Check for updates

Heze Zhang[1,6], Chao Zeng[1,6], Yueqing Du[1], Guanghua Cheng[2], Biqiang Jiang[1], Zhipei Sun[3], Xuechun Lin[4], Meng Pang[5], Jianlin Zhao[1] & Dong Mao[1]

Multi-pulse oscillations are prevalent phenomena observed in mode-locked lasers and nonlinear microresonators, where the short- and long-range interactions between nonlinear wavepackets give rise to diverse pulse patterns such as soliton molecules, soliton crystals, and soliton bursts. However, these intricate nonlinear interactions are highly sensitive to the parameters of dissipative systems, leaving the properties of multiple pulses far from being controlled, which hampers their applications such as high-speed optical communication and material processing. In this study, we propose a universal approach for quantitatively tailoring multiple solitons in mode-locked fibre lasers through spectral phase programming, enabling the on-demand generation of soliton patterns with separations that follow from constant, geometric, or arithmetic sequences. By combining with spectral filtering, we demonstrate dual-colour soliton patterns in the same cavity, further highlighting the adaptability of soliton structures. Numerical simulations validate the experimental observations, demonstrating that the spectral phase modulates solitons to emit sub-pulses, which interact with other solitons to generate trapping potentials, thereby giving rise to diverse soliton patterns.

Ultrashort laser pulses, comprising coherent electric field envelopes with durations as short as femtoseconds, serve as fundamental building blocks in nonlinear physics and ultrafast science[1–4]. The pursuits of improving frequency stability, enhancing pulse intensity and minimising pulse width have driven the advancement of various state-of-the-art technologies such as optical frequency comb[5–7], chirped-pulse amplification[8,9] and attosecond pulse generation[10,11]. Attributing to the over-accumulated nonlinear phase shift, the mode-locked lasers usually transform from single-pulse operation to a multi-pulse state at high pump levels, which is particularly pronounced for fibre lasers and nonlinear microresonators due to their strong nonlinearity and confined mode field area[12–14].

In the presence of slow gain dynamics, the multiple pulses in a fibre laser can be arranged into evenly spaced sequences with typical separations on the order of nanoseconds[15], resulting in the so-called harmonic mode locking[16]. Concerning the closely spaced multiple pulses within the cavity, the short-range interactions automatically assemble them into diverse patterns, commonly referred to as soliton molecules[17–19], soliton fluids[20], and soliton crystals[13], analogous in many ways to their matter counterparts formed by covalent bonds. Specifically, the short-range interactions occur through the cross-phase modulation effect when multiple solitons directly overlap in their tailing fields[21,22], forming soliton molecules

[1]Shaanxi Key Laboratory of Optical Information Technology, Key Laboratory of Light Field Manipulation and Information Acquisition, Ministry of Industry and Information Technology, School of Physical Science and Technology, Northwestern Polytechnical University, Xi'an 710129, China. [2]School of Electronics and Information, Northwestern Polytechnical University, Xi'an 710021, China. [3]Department of Electronics and Nanoengineering and QTF Centre of Excellence, Aalto University, Aalto, Espoo, Finland. [4]Laboratory of All-solid-state Light Sources, Beijing Engineering Research Center, Institute of Semiconductors, Chinese Academy of Sciences, 100083 Beijing, China. [5]State Key Laboratory of High Field Laser Physics, Shanghai Institute of Optics and Fine Mechanics, Chinese Academy of Sciences, Shanghai 201800, China. [6]These authors contributed equally: Heze Zhang, Chao Zeng. e-mail: maodong@nwpu.edu.cn

with fixed phase relations or intriguing internal dynamics characterised by vibrating separation and sliding phase[23,24]. When the separations between solitons are tens to hundreds of times their durations[25,26], various physical mechanisms, including perturbation-induced effects[27], optoacoustic interactions[28–30], Casimir-like effect[15], and thermal effect[31], are responsible for the long-range interactions. Due to the high sensitivity of these complex nonlinear interactions to the parameters of dissipative systems, the quantitative manipulation of multiple pulses in mode-locked lasers has proven to be a significant challenge.

Currently, various active approaches such as gain/loss management[32–35] and polarisation optimisation[36,37] have been developed to control the soliton distributions, with the majority of studies focused on two solitons. The gain modulation influences the interaction potential of two solitons, resulting in the rapid switching of soliton separation among several discrete values[32,33]. By introducing the filtering effect into the cavity[34], the separation between two solitons can be tailored from 3.014 to 5.478 ps, whereas the soliton properties vary obviously due to the inevitable loss. With the aid of an evolutionary algorithm and a real-time feedback system, it becomes feasible to achieve a predetermined separation of two solitons through a computational process lasting several seconds[36,37]. The distributions of such solitons are indirectly controlled through manipulating pulse characteristics such as intensity and polarisation state, and thereby it is difficult to establish a direct functional relationship between control parameters and pulse separations.

For multiple solitons (≥3), the attractive and repulsive forces among them exhibit a significantly intricate nature, often resulting in equally spaced interaction potentials[14]. Thus, the active control of pulse distributions, particularly for multiple solitons with unequal distributions, still remains a significant challenge impeding their widespread applications in all-optical logic gate[38], high-speed communication[39] and data storage[29]. In this study, we propose a universal approach to quantitatively tailor soliton patterns with arbitrary distributions by programming the spectral phase inside a fibre laser. The spectral phase modulation enables the formation of discrete sub-pulses on soliton tails, following from the Fourier transform shift theorem. The overlapping and interaction between these sub-pulses and solitons give rise to multiple potential wells in the cavity, capable of trapping solitons at predetermined positions. As a demonstration, we achieve the on-demand generation of soliton patterns with separation following from constant, geometric, and arithmetic sequences, as well as dual-colour soliton patterns.

Results

Principle and setup

According to the Fourier transform shift theorem, the introduction of a linear spectral phase in the spectrum leads to a delay of the pulse in the time domain[40,41]. As depicted in the upper panel of Fig. 1a, a weak pulse is formed by imparting a linear spectral phase to the pulse spectrum, where the temporal separation between two pulses depends on the slope of the linear phase. The 2D colour plots represent the spectrograms of the pulse, which are derived from the short-time Fourier transform of the pulse electric field.

By programming the spectral phase on a pulse, such as imparting periodic triangular phases $\varphi(\nu)$, specific portions of the spectra can be extracted in the time domain, manifesting as several peaks on the spectrogram, as depicted in the middle panel of Fig. 1a. These spectral components give birth to a sequence of sub-pulses at positions of constructive interference. The triangular phase with a period of Λ can be expressed as:

$$\varphi(\nu)=\begin{cases}0, (n-1)\Lambda<\nu\le n\Lambda-\delta\nu\\ 2\pi\tau[\nu-(n\Lambda-\delta\nu)], n\Lambda-\delta\nu<\nu\le n\Lambda\end{cases}, \quad (1)$$

where the integer n corresponds to the order of the sub-pulses, ν denotes the frequency, τ represents the group delay, and $\delta\nu$ is the bandwidth of the phase. As the amplitude of the triangular phase $2\pi\tau\delta\nu$ (<0.3 rad) is significantly smaller than that of the original phase (5–8 rad)[42], the pulse intensity $I(t)$ after introducing the periodic triangular phase can be analytically expressed as follows (see derivation details in Supplementary Note 1):

$$I(t)\approx I_0(t)+\sum_{n=-\infty}^{\infty}\frac{\tau(\delta\nu)^2}{(9.8\pi)^2\Lambda\sqrt{|n|}}I_0\left(t-\frac{n}{\Lambda}\right),\ n=(\pm1,\pm2,\cdots). \quad (2)$$

Here, the first term on the right-hand side represents the primary pulse, whereas the second term denotes the sub-pulses. The intensities of sub-pulses are directly proportional to the bandwidth of phase modulation $\delta\nu$ and rapidly decrease as the order of the sub-pulses n increases.

It is worth mentioning that, the separations between sub-pulses are determined by the reciprocal of the phase period Λ, and are independent of the group delay τ. Consequently, the characteristics of sub-pulses, particularly their distributions, can be quantitatively controlled via the triangular spectral phases or their superposition (lower panel of Fig. 1a). Because τ is much smaller than $1/\Lambda$, the sub-pulses almost appear symmetrically on both sides of the primary pulse.

The periodic triangular spectral phase, as described by Eqs. 1, 2, introduces seed pulses into the cavity, which gradually evolve into solitons under the coaction of gain, loss, dispersion, saturable absorption, and nonlinearity. When multiple solitons co-propagate within the cavity, the periodic spectral phase modifies each soliton, generating discrete sub-pulses on soliton tails. The overlapping and interaction between sub-pulses and solitons give rise to multiple potential wells, resulting in tailored soliton patterns with on-demand separations (Fig. 1b).

In the experiment, we construct a mode-locked erbium-doped fibre laser to demonstrate our proposal and generate the desired soliton patterns. The laser cavity is comprised of a wavelength-division multiplexer, a 6-m erbium-doped fibre, a polarisation-insensitive isolator, a 90:10 optical coupler, a carbon nanotube saturable absorber, and a programmable pulse shaper. The carbon nanotube saturable absorber initiates the mode-locking operation, and the programmable pulse shaper imparts the spectral phase and filtering into the cavity. The cavity length and net cavity dispersion are 18.9 m and −0.52 ps^2, respectively. The details of the laser configuration and measurement system are provided in Supplementary Note 2.

Dual-pulse soliton patterns

The fibre laser initially delivers a single chirp-free soliton at a pump power of ~30 mW due to the balance between the anomalous dispersion and self-phase modulation effects[43] (Supplementary Note 3). The soliton number increases one by one when elevating the pump power in steps of ~5 mW. However, the distributions of multiple solitons are random and change irregularly with the pump power, polarisation state, and environmental perturbations. After incorporating the periodic triangular spectral phases into the cavity, the potential wells are established in the fibre laser, thereby enabling the generation of controllable soliton patterns.

As one of the simplest verifications, dual-pulse soliton patterns are obtained at a pump power of 35 mW using periodic triangular spectral phases depicted in Fig. 2a. In this case, the group delay τ and bandwidth $\delta\nu$ of phase remain unchanged at 0.5 ps and 0.006 THz (0.048 nm), respectively, whereas the phase period decreases from 0.2 to 0.015 THz (1.61 to 0.12 nm); thus, the separation of the spectral phase-associated potential wells increases from 5 to 66.67 ps. As shown in Fig. 2a–d, the modulation period in the spectrum almost equals that of the spectral phase, and the soliton separations (marked by the red dots in Fig. 2b) are governed by the spectral phase-

https://doi.org/10.1038/s41467-025-59990-x

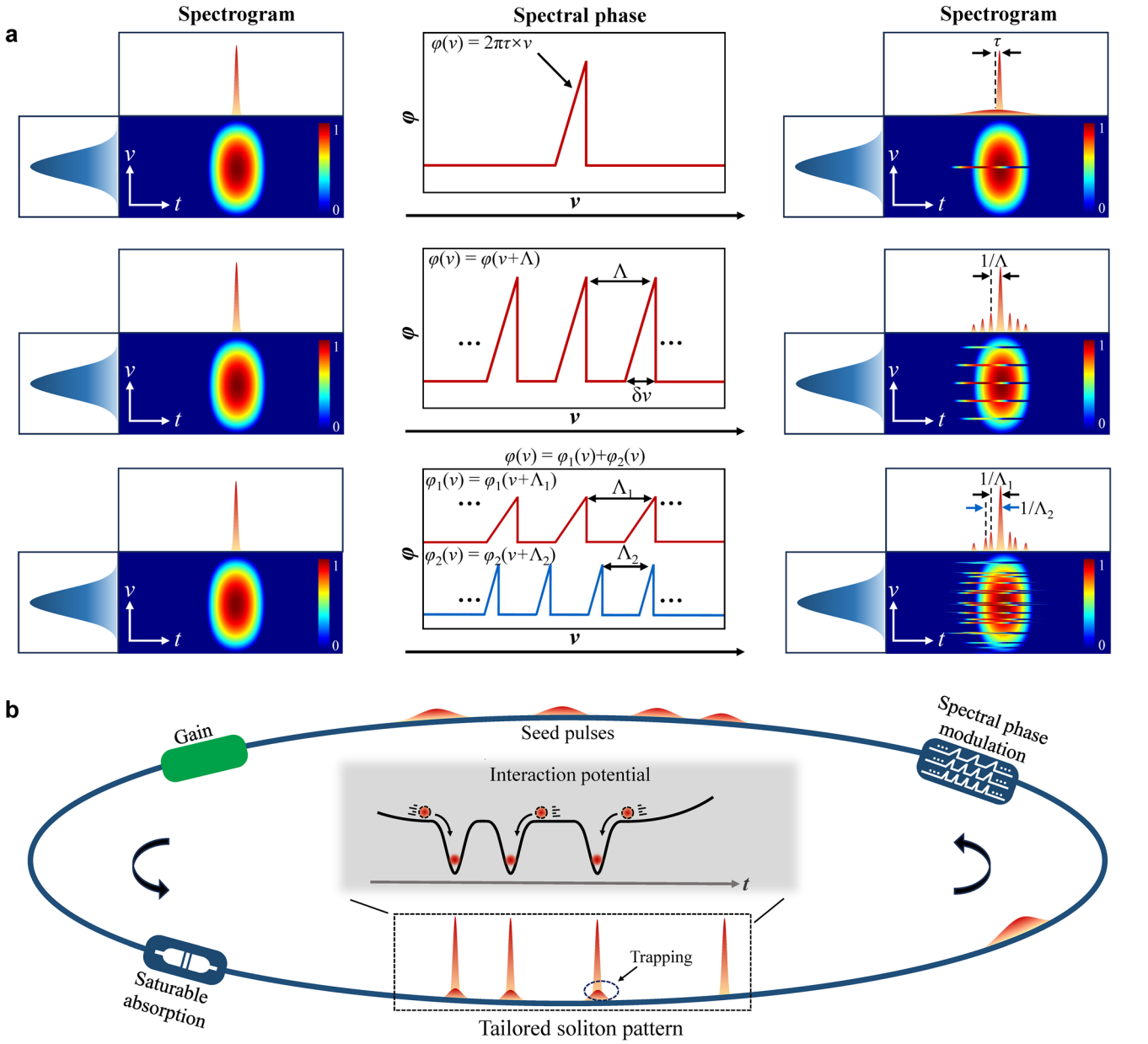

Fig. 1 | Conceptual illustration of tailoring soliton patterns via intracavity phase programming. a Sub-pulses are formed when imparting triangular spectral phases to the pulse spectrum. **b** Spectral phase modulation introduces seed pulses into the cavity, which evolve into robust solitons that are trapped by potential wells arising from the overlapping between sub-pulses and other solitons, resulting in tailored soliton patterns.

associated potential wells, increasing from 4.31 to 66.51 ps. Moreover, the same dual-pulse soliton pattern can be obtained by imparting spectral phases with different values of group delay τ, coinciding with Eq. 2 that the separations of sub-pulses are independent with τ. The experimental results support the theoretical predictions, suggesting that spectral phase modulation is the primary factor in distributing pulses within soliton patterns (see Fig. 2c).

The spectral phase-associated potential wells endow soliton patterns with remarkable resilience to perturbations in experimental conditions. For example, the fibre laser maintains the same mode-locked state throughout the entire experiment, with a variation in soliton separation of less than 0.06 ps (over 1 ms) and 0.3 ps (over 12 h) (see details in Supplementary Note 4). The pronounced modulations in the spectra and the high signal-to-noise radio frequency spectrum (Fig. 2d) also provide compelling evidence for the stability of the soliton pattern. By removing spectral phase modulation, however, the double soliton exhibits stochastic attraction and repulsion before ultimately assembling into a new soliton pattern (Fig. 2e), which further validates that the trapping effect is dominated by the spectral phase modulation.

Based on the lumped propagation model and the generalised nonlinear Schrödinger equation[44,45], we conduct numerical simulations to elucidate the formation mechanism of the soliton patterns, in which the spectral phase is particularly considered by multiplying the optical field with the phase function in the frequency domain. The equation and simulation parameters are described in the "Methods" section.

Figure 3a depicts the build-up process of the double soliton with a phase period of 0.056 THz and a gain saturation energy of 165 pJ. Attributing to the periodic triangular phase modulation, the initial weak pulse gradually evolves into multiple seed pulses after 40 roundtrips, with a separation of 18 ps, coinciding with the theoretical value derived from Eq. 2. Meanwhile, the modulation structure

https://doi.org/10.1038/s41467-025-59990-x

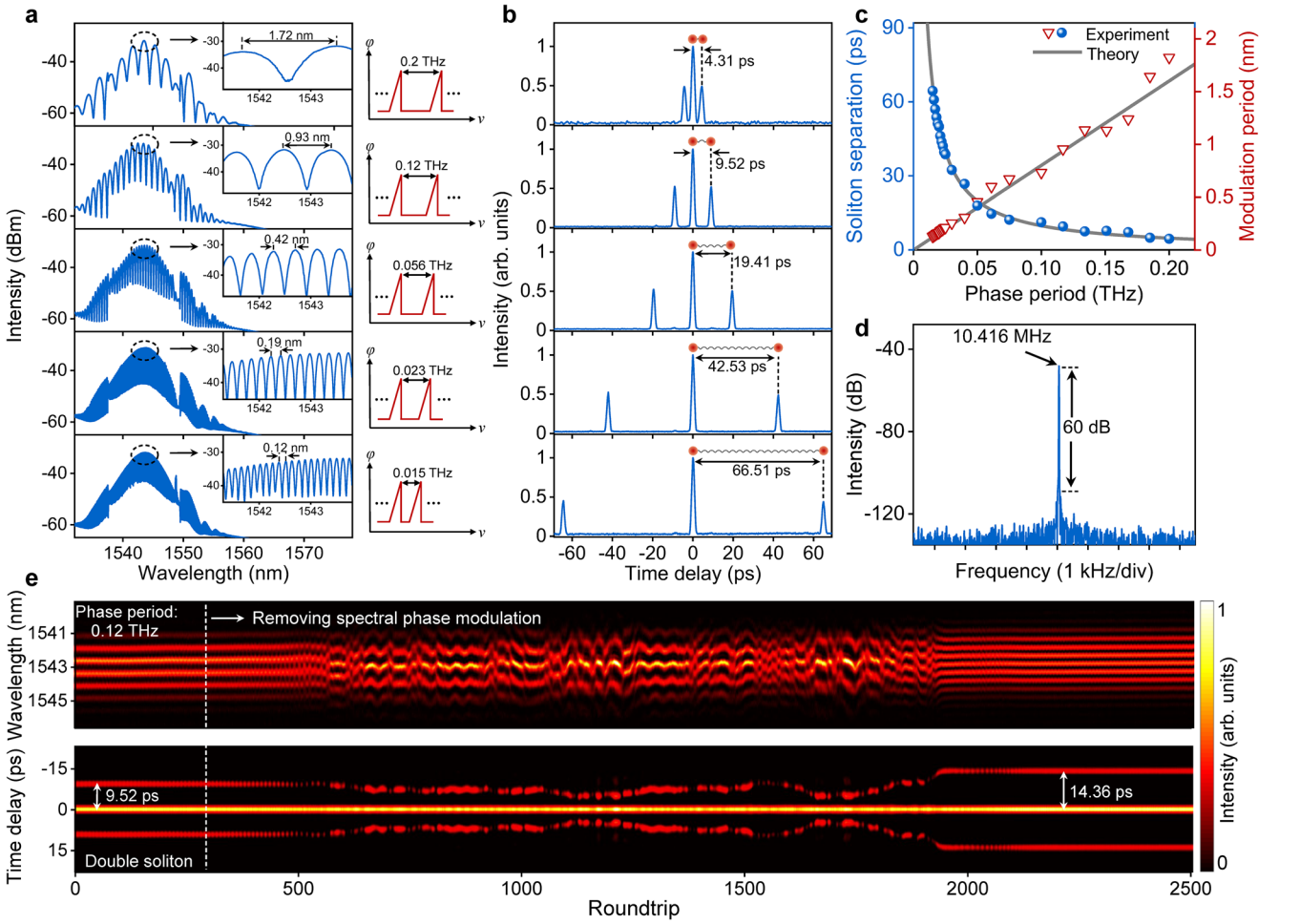

Fig. 2 | Dual-pulse soliton patterns. a Spectra and (**b**) autocorrelation (AC) traces under different phase periods. **c** Soliton separation and spectral modulation period versus phase period. **d** Radio frequency spectrum for phase period of 0.056 THz. **e** Evolutions of the real-time spectrum and field AC trace by removing the spectral phase modulation at roundtrip 300, marked by the white dashed line.

emerges on the spectrum because of the interference between the multiple seed pulses. Afterwards, the separation of seed pulse converges to a constant value due to the spectral phase-associated potential wells. During this process, two seed pulses grow into robust solitons through the coaction of gain, self-phase modulation, anomalous dispersion, and saturable absorption. Consequently, double solitons with a separation of 19.53 ps are formed in the simulation, which closely aligns with the experimental findings (Fig. 2b: 19.41 ps).

The build-up process of double solitons differs from that in the previous study, where the gain-loss dynamics govern the soliton splitting and soliton interaction processes before reaching the steady state[46]. By eliminating spectral phase modulation in the simulation, the seed pulses vanish during the build-up process, and the soliton separation markedly diverges from the theoretical prediction, thereby underscoring the essential role of spectral phase modulation in pulse formation and soliton trapping (Supplementary Note 5).

It is worth noting that the soliton separations mentioned above slightly deviate from the theoretical prediction (18 ps) based on the Fourier transform principle (Eq. 2). By varying the cavity dispersion from −0.65 to −0.02 ps^2, we study the evolution of double solitons with cavity dispersion under the same phase period of 0.056 THz (Fig. 3b). The soliton separation deviates from the theoretical prediction in the anomalous dispersion regime (grey region), and converges to approximately 18 ps in the near-zero dispersion regime (green region). This phenomenon can also be verified in the experiment by tuning the cavity dispersion from −0.52 to −1.52 ps^2 (Supplementary Note 6).

As evidenced by the experimental and simulated demonstrations, such deviation is primarily attributed to the cavity dispersion. In anomalous-dispersion fibre lasers, the solitons are perturbed and release energies in the form of dispersive waves, giving birth to oscillating tails under the phase-matching condition[47]. As these perturbed solitons co-propagate within the laser cavity, they interact through their oscillating tails and also induce potential wells, compelling each soliton to align with the peaks of oscillations[27]. In the near-zero dispersion regime, the phase-matching condition is harsher to be satisfied within the gain bandwidth of the laser. As a result, the potential wells induced by dispersive waves become much weaker, thereby reducing the deviation in soliton separation.

The effective potential can be calculated in terms of the integrals of overlapping between separated solitons[17]. In our scheme, the spectral phase modulation imparts solitons with sub-pulses on tails, whose intensities are significantly larger than those induced by dispersive waves (Fig. 3c). We utilise two solitons to calculate the effective potential as a function of soliton separation (see details in Method and Supplementary Note 7). As illustrated in Fig. 3d, the red dashed circles denote potential wells originating from spectral phase modulation, with depths much larger than those induced by dispersive waves (black dashed boxes). These results confirm that spectral phase modulation can create potential wells within the cavity, enabling the effective trapping of solitons. Moreover, the properties of potential wells can be flexibly controlled by the spectral phase parameters and relative phase between two solitons (Supplementary Note 8).

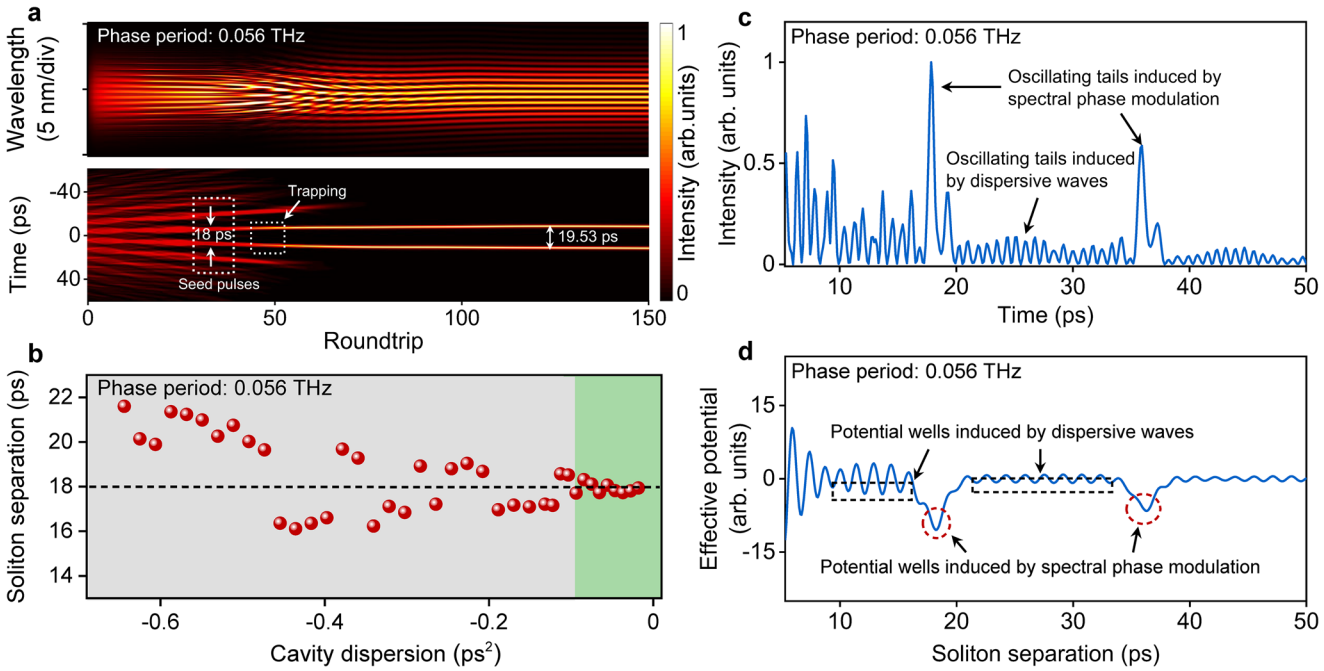

Fig. 3 | Simulations of dual-pulse soliton patterns. a Build-up process. **b** Soliton separation versus cavity dispersion. The dashed line denotes the theoretical separation derived from Eq. 2 for $\Lambda = 0.056$ THz. **c** Profiles of soliton tails. **d** Evolution of effective potential with soliton separation.

Soliton patterns with constant sequence separations

As a periodic triangular spectral phase creates many equally spaced potential wells, multiple solitons with constant separations can be obtained in the fibre laser by solely elevating the pump power. Figure 4a, b shows the spectra and autocorrelation (AC) traces of such soliton patterns for the same phase period of 0.056 THz as that in Fig. 2. The soliton number increases one by one with the enhancement of pump power while the solitons are trapped by the spectral phase-associated potential wells, with separations spanning from 19.13 to 19.15 ps, also comparable with the theoretical prediction of 18 ps. By solely increasing the phase period to 0.083 THz, the soliton separation is reduced to approximately 12 ps (Supplementary Note 9), further validating that the distribution of multiple solitons primarily relies on the spectral phase.

The simulation results agree with the experimental observations, wherein by increasing the gain saturation energy to 235 and 380 pJ, triple and quadruple solitons with constant separations are established respectively (Fig. 4c–f). The build-up processes resemble that of the double solitons, both involving the transformation of the seed pulses into robust solitons and the trapping process. The separations of seed pulses are equal to the reciprocal of the phase period (18 ps), highlighting the crucial role of spectral phase modulation in generating soliton patterns with constant sequence separations. The presence of such soliton patterns suggests the potential for generating soliton crystals under sufficient gain and nonlinearity.

Soliton patterns with geometric/arithmetic sequence separations

The key to tailoring multi-pulse soliton patterns involves the precise manipulation of sub-pulses and spectral phase-associated potential wells. According to the Fourier transform principle, the superposition of spectra with multiple periodic triangular spectral phases generates sub-pulses exhibiting unequal separations due to interference (lower panel of Fig. 1a). This, in turn, leads to unequally spaced potential wells that trap solitons, thereby facilitating the generation of multiple solitons with arbitrary distributions.

We first demonstrate quadruple solitons with geometric sequence separations in the fibre laser (Fig. 5a–d), where the spectral phase exhibits three distinct periods: 0.1, 0.033, and 0.014 THz, corresponding to sub-pulse separations of 10, 20, and 40 ps, respectively (the detailed parameters of the spectral phase are provided in Supplementary Note 2). Owing to the interference of multiple solitons with unequal separations, the spectrum displays intricate beating fringes while the envelope features a quasi-Sech^2 profile, a typical fingerprint of solitons in anomalous-dispersion regime (Fig. 5b). By incorporating the frequency control actuator into the cavity[48], the mode-locked fibre laser may generate a customised optical frequency comb on demand.

Unlike equally spaced solitons, the AC traces show gradually decreasing multi-peak structures (Fig. 4b), the AC trace in Fig. 5c displays one main peak and multiple side peaks, from which the pulse distribution in the soliton pattern can be extracted based on the autocorrelation theory[49] (see details in Supplementary Note 10). As shown in Fig. 5d, the soliton pattern is composed of four pulses with separations of 10.36, 22.29, and 42.02 ps, which correspond to the most prominent sub-pulses induced by the spectral phase (indicated by the green triangles).

Keeping the other parameters unchanged, quintuple solitons with arithmetic sequence separations can also be obtained by imparting four periodic triangular spectral phases into the cavity (the phase periods are 0.1, 0.04, 0.022, and 0.014 THz). As shown in Fig. 5e–h, the soliton separations extracted from the AC traces are 12.19, 17.37, 20.75, and 23.52 ps, which are comparable with the theoretical values of 10, 15, 20, and 25 ps, respectively. The pulse number and separation of these soliton patterns can be flexibly manipulated by changing the pump levels and phase periods. For example, we successfully generated quadruple solitons with separations following the arithmetic sequence in the same fibre laser (Supplementary Note 11).

We further simulate the build-up process of the quadruple solitons with geometric sequence separations (Fig. 5i–l). Starting with a weak pulse, the spectral phase first induces multiple seed pulses with unequal separations inside the cavity before 50 roundtrips. Then the seed pulses undergo complex soliton interactions, including drift and

https://doi.org/10.1038/s41467-025-59990-x

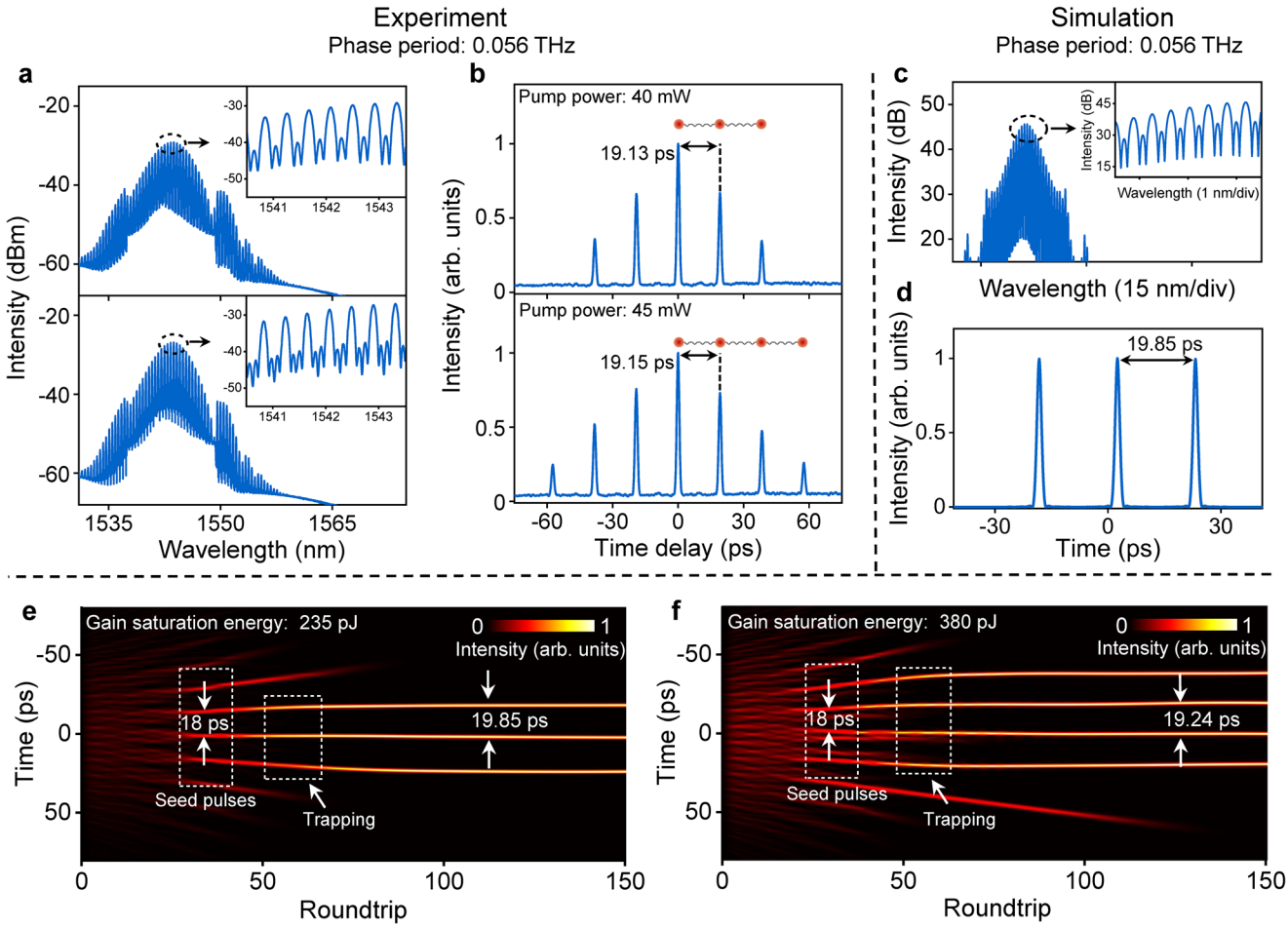

Fig. 4 | Soliton patterns with constant sequence separations. Experiment: **a** spectra and (**b**) AC traces. Simulation: **c** Spectrum and (**d**) soliton pattern. Build-up processes of (**e**) triple and (**f**) quadruple solitons.

collision. After that, the pulse splits and is trapped by the spectral phase-associated potential wells, ultimately reaching a steady state. For free-running multiple solitons, the mutual interactions among them usually lead to various evolution dynamics, such as sliding and oscillating phase[50]. However, the phase relations among multiple pulses in soliton patterns nearly remain unchanged, indicating the robustness of such soliton structure.

The soliton separations (i.e. 12.76, 22.58 and 36.1 ps) are comparable to the theoretical values, confirming the validity of the phase programming approach for generating soliton patterns with arbitrary distributions. The deviations from the theoretical predictions also stem from the dispersion-associated potential wells—such deviation becomes less evident in a near-zero dispersion fibre laser, wherein an ideal geometric sequence soliton pattern can be established with the same phase modulation (Supplementary Note 12, the pulse separations are 10.24, 20.06 and 39.61 ps).

Our results indicate that each pulse in these soliton patterns corresponds to the first-order potential wells induced by the periodic triangular spectral phase. This can be deduced from Eq. 2 that the sub-pulses for $n = \pm 1$ exhibit the highest intensities. The combined influence of gain competition, saturable absorption, and slow gain dynamics could shape the leading sub-pulse ($n = -1$) into a soliton while other sub-pulses undergo gradual decay during circulation within the cavity.

In principle, soliton patterns with arbitrary distributions can be achieved through the phase programming approach. However, the limited resolution of the programmable pulse shaper (0.001 THz) results in a minimum phase period of 0.002 THz, thereby restricting the maximum soliton separation to less than 500 ps. The utilisation of dielectric metasurface[51] or electro-optic modulator[25] may support soliton patterns with more distant separations. When the ratio between soliton separation and duration is less than ~5, the short-range interaction[17,18] becomes comparable to the spectral phase-associated trapping effect, and both dominate the characteristics of soliton patterns. This implies a prospective avenue to investigate the interaction force between closely spaced solitons through the phase programming approach.

Dual-colour soliton patterns

By simultaneously imparting the periodic triangular phases and parabolic phases into the cavity, the proposed fibre laser can also generate dual-colour soliton patterns with on-demand separations both in the time and frequency domains, aided by a double-channel band-pass spectral filter. Figure 6a–h depicts the properties of the measured and simulated dual-colour soliton patterns. The phase profiles are shown in Fig. 6a, e, in which the parabolic phase enables the synchronisation of solitons at different wavelengths, and the periodic triangular phase (the zoom-in of Fig. 6a, e) facilitates the generation of potential wells to trap solitons. In fact, the dual-colour soliton patterns consist of four elementary pulses. In each mode-locked spectrum, two pulses form a soliton molecule with a separation of 48.02 ps due to the influence of the periodic triangular phase. With the aid of the group-delay compensation induced by the parabolic phase and saturable absorption[52], two soliton molecules at 1540.85 and 1545.93 nm are synchronised and overlapped in the time domain, forming a dual-colour pattern with modulated structures.

https://doi.org/10.1038/s41467-025-59990-x

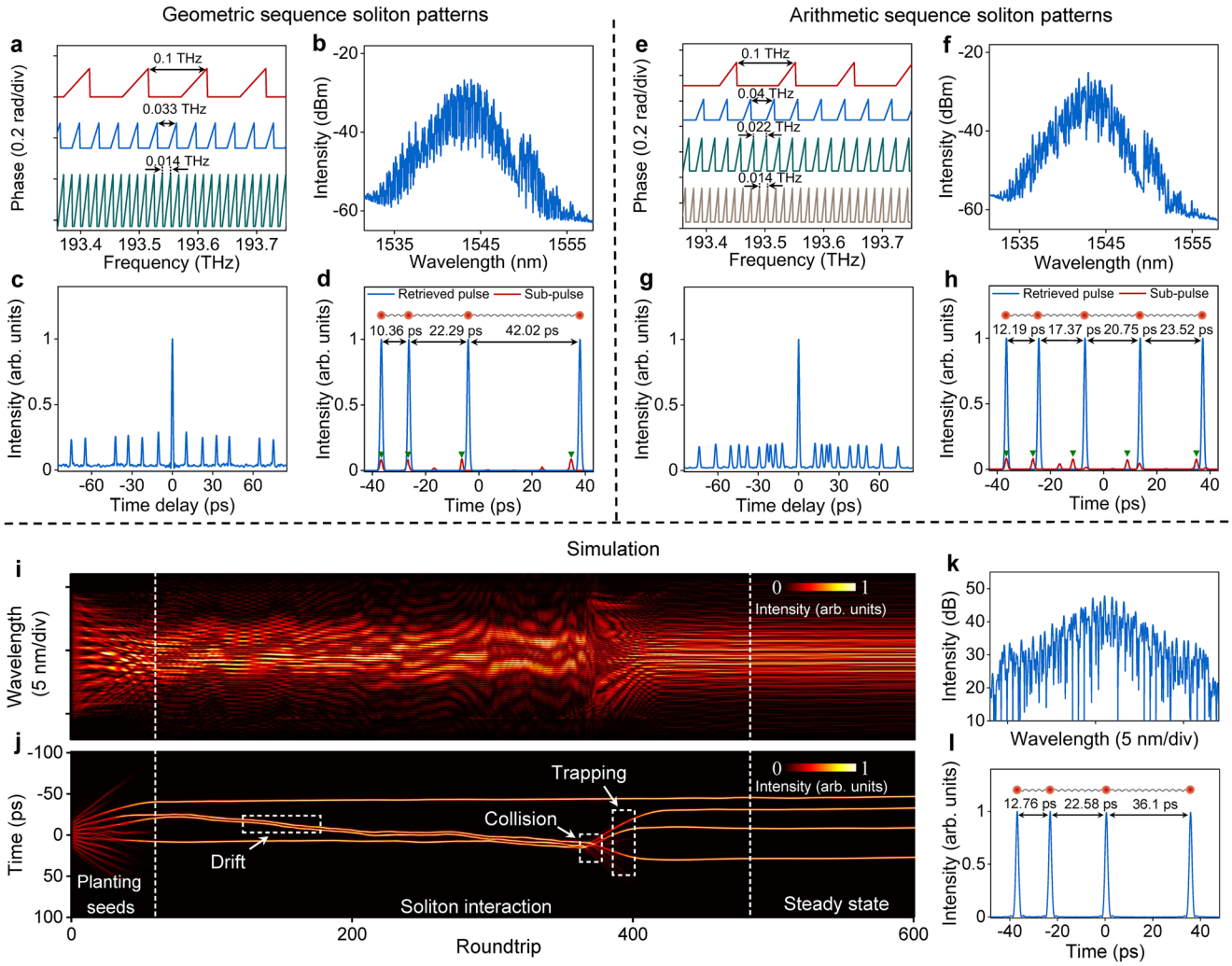

Fig. 5 | Soliton patterns with geometric and arithmetic sequence separations. a, **e** Spectral phases. **b**, **f** Spectra. **c**, **g** AC traces. **d**, **h** Distributions of soliton patterns and sub-pulses. Simulation: **i**, **j** Build-up process of quadruple solitons with geometric sequence separations. **k** Spectrum and **l** soliton pattern in the steady state.

The formation of dual-colour soliton patterns includes pulse stretching, narrowing, splitting, and trapping (Fig. 6i, j), in which the chromatic dispersion, nonlinear effect, gain, and spectral phase-associated potential wells dominate the four processes, respectively. It is worth noting that, the separations of wavepackets in dual-colour soliton patterns can be tuned over a wide range without affecting other pulse properties such as wavelength spacing and wavepacket width (Supplementary Note 13).

The wavelength number of dual-colour soliton patterns could be increased by imparting multiple parabolic phases and spectral filtering into the cavity. As the spectrum is confined by the spectral filter, the wavepacket width can be flexibly adjusted by tuning the filtering bandwidth due to the transform-limited nature of the soliton. In this regard, the utilisation of phase programming in conjunction with spectral filtering provides a multi-dimensional approach to tailor soliton patterns in both the frequency and time domains. Such unique dual-colour soliton patterns not only provide a profound analogy with complex molecular compounds in chemistry, such as H_2O_2 and C_2H_2, but also hold significant potential in the fields of ultrafast spectroscopy[53] and dual-comb ranging[54].

Discussion

We have demonstrated a universal approach for tailoring soliton patterns in a mode-locked fibre laser. By programming the spectral phase within the cavity, the temporal distribution and spectral properties of solitons can be quantitatively manipulated, giving birth to a variety of elegant soliton patterns. The experimental observations are fully reproduced and explained by numerical simulations, showing that the periodic spectral phase modifies solitons to form sub-pulses on their tails. The overlapping and interaction of sub-pulses with other solitons results in multiple potential wells for soliton trapping, thereby giving rise to the soliton patterns with customised distributions, under the synergistic interplay among gain, anomalous dispersion, saturable absorption, and nonlinearity.

Previous studies on the manipulation of soliton patterns have focused on two solitons[32–34,36,37]. The phase programming approach overcomes this limitation by introducing multiple sub-pulses into the laser cavity, enabling the quantitative tailoring of soliton patterns with arbitrary temporal distributions and spectral morphologies. In contrast to the spectral filtering method[36], the phase programming approach enables the manipulation of multiple solitons without introducing any filter loss into the cavity.

The temporal phase modulation approaches, such as electro-optic modulation[25] and optomechanical interaction[29], create trapping potentials by modifying the instantaneous frequencies of solitons, capable of forming soliton patterns with equal separations. In contrast, spectral phase modulation enables the formation of soliton patterns with arbitrary distributions, and such a scheme does not require the locking between the phase period and free spectral range of the cavity.

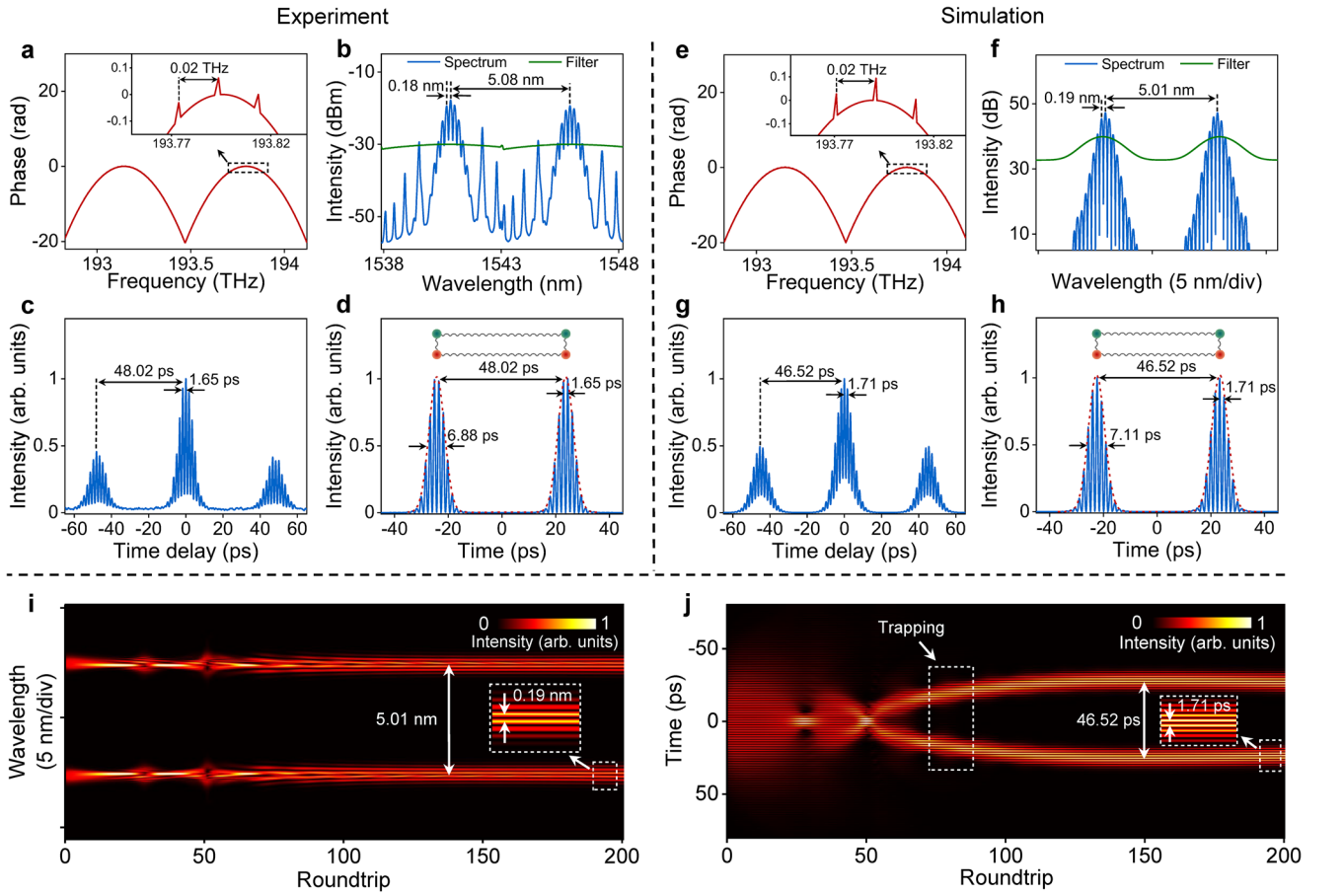

Fig. 6 | Dual-colour soliton patterns. a, **e** Spectral phases. **b**, **f** Spectra and filter traces. **c**, **g** AC traces. **d** Wavepackets extracted from the AC trace and (**h**) obtained in the simulation. **i**, **j** Build-up processes.

By incorporating photonic crystal fibres into the laser cavity, the coaction of optomechanical interaction and spectral phase modulation may permit the generation of highly ordered soliton patterns with customised separations[29,30], further extending the light-matter molecular analogy and enriching the physics of the laser system. Thus, the proposed laser can serve as an ideal platform for exploring new types of nonlinear wavepackets and understanding their evolution dynamics, with significant potential in communications[55] and all-optical switching[33].

Previous studies have demonstrated that the temporal parabolic potential can stabilise the oscillatory and chaotic dynamics[56], favoring the formation of static dissipative Kerr solitons. Given that the trapping potentials induced by soliton tails have been utilised to effectively control chaotic soliton bunches[57], our scheme holds great promise for mitigating chaotic dynamics in coherently driven passive cavities, generating novel dissipative structures such as asymmetric breathers and chimera-like states[58], and exploring Bloch oscillations in a synthetic frequency dimension[59].

The proposed scheme exhibits remarkable versatility beyond fibre lasers, demonstrating the promising potential for application in other nonlinear systems capable of supporting multi-pulse oscillations, such as microresonators[60,61] and solid-state lasers[62]. Recent report has demonstrated that the periodic potential field generated by the dual pumps enables the on-demand synthesis of soliton crystals[63]. In this regard, our proposal holds great promise for tailoring soliton patterns in microresonators with enhanced flexibility, thereby forming intricate frequency combs for specific applications. Note that the relative phase between two solitons can be actively manipulated by tuning the pump power[64], further investigation can focus on the joint manipulation of the distribution and phase of multiple solitons.

From an application perspective, the fibre laser can generate soliton patterns with arbitrary distributions, which is particularly attractive in laser processing as such pulses could provide higher ablation efficiency and machining accuracy than a single one[65,66]. Specifically, the soliton pattern with different separations presents a viable option for non-reciprocal ultrafast laser writing[67]. The phase programming approach also provides a feasible avenue for data encoding and optical storage. For example, the information 'NPU' can be written into the cavity through tailoring quadruple soliton patterns (Supplementary Note 14).

Methods

Simulation model

The numerical simulation is based on the lumped propagation model, where each component is modelled by a transmission function[45]. After one circulation, the output pulse is utilised as the input for the subsequent roundtrip until the laser reaches a self-consistent state. During propagation in passive fibre and gain fibre, the pulse is governed by the generalised nonlinear Schrödinger equation incorporating gain, loss, dispersion, and Kerr nonlinearity[19]:

$$\frac{\partial u}{\partial z} = -i\frac{\beta_2}{2}\frac{\partial^2 u}{\partial t^2} + i\gamma|u|^2u + \frac{(g-\alpha)}{2}u + \frac{g}{2\Omega_g^2}\frac{\partial^2 u}{\partial t^2} \quad (3)$$

Here, u represents the slowly varying envelope of the pulse, t and z are the time and propagation distance, respectively. γ is the cubic refractive nonlinearity and β_2 denotes the second-order dispersion

coefficient of fibres. g, α, and Ω_g represent the gain, loss, and gain bandwidth, respectively. For the erbium-doped fibre, $g = g_0 \exp(-E_p/E_s)$, in which g_0, E_p, and E_s are the small-signal gain coefficient, pulse energy, and gain saturation energy, respectively. The transmittance function of the saturable absorber is $T_{SA} = 0.46 - T_0/[1 + P_{(t)}/P_{sat}]$, where T_0, $P_{(t)}$, and P_{sat} denote the modulation depth, instantaneous pulse power, and saturable power, respectively. The typical split-step Fourier method is employed to solve this equation[68].

The programmable pulse shaper imparts spectral phase and spectral filtering into the cavity, which is modelled by multiplying the optical field with the corresponding function in the frequency domain. The function of the periodic triangular phase is depicted in Eq. 1. The two parabolic phases exhibit identical profiles but differ in their central frequencies. Each parabolic phase is modelled by $\varphi_P(\nu) = A(\nu - \nu_c)^2/4\pi^2$, where A and ν_c represent the group-delay dispersion and central frequency, respectively. The transmittance function of the filter is:

$$T(\nu) = \frac{1}{2}e^{\frac{-4\ln 2(\nu-\nu_0)^2}{B^2}} + \frac{1}{2}e^{\frac{-4\ln 2(\nu-\nu_1)^2}{B^2}} + \frac{1}{10}, \tag{4}$$

where B is the filtering bandwidth, ν_0 and ν_1 represent two central frequencies of double-channel band-pass spectral filter. The spacing between two passbands (i.e. $\nu_0 - \nu_1$) is the same as that of two parabolic phases.

The simulation parameters are set as follows to match the experiments: $T_0 = 0.08$, $P_{sat} = 10$ W. For the single-mode fibre, $\alpha = 4.6 \times 10^{-5}\,m^{-1}$, $\beta_2 = -21.7\,ps^2\,km^{-1}$, $\gamma = 1.3\,W^{-1}\,km^{-1}$. For the programmable pulse shaper, $\beta_2 = -120.3\,ps^2\,km^{-1}$, $\gamma = 0$. For the erbium-doped fibre, $g_0 = 0.7\,dB\,m^{-1}$, $\beta_2 = 21.3\,ps^2\,km^{-1}$, $\gamma = 3.9\,W^{-1}\,km^{-1}$. For the double solitons in Fig. 3, $E_s = 165$ pJ, the parameters of the triangular phase $(\Lambda; \tau; \delta\nu)$ is (0.056 THz; 0.5 ps; 0.006 THz). For the triple and quadruple solitons in Fig. 4, E_s are 235 and 380 pJ, respectively. The other parameters are the same as that of double solitons. For the geometric sequence soliton pattern in Fig. 5, $E_s = 165$ pJ. The imparted triangular phase contains three functions with parameters: $(\Lambda; \tau; \delta\nu)$ = (0.1, 0.033, 0.014 THz; 0.5, 1.5, 7.5 ps; 0.045, 0.014, 0.0085 THz). For the dual-colour soliton pattern in Fig. 6, $E_s = 350$ pJ, $A = -4.943\,ps^2$, $B = 0.201$ THz, $\nu_0 - \nu_1 = 0.641$ THz, $\delta\nu = 0.0025$ THz, $\tau = 3$ ps, $\Lambda = 0.02$ THz.

Calculation of effective potential

In the context of a perturbed nonlinear Schrödinger equation, the interaction of slightly overlapping solitary pulses enables the formation of two- and multi-pulse bound states[17]. The effective potential can be calculated in terms of the integrals of overlap between separated solitons. For the two solitons separated by Δ, the effective potential U between them can be approximately expressed as (see details in Supplementary Note 7):

$$U(\Delta) = -4\int_{-\infty}^{+\infty} |u_1(t)|^2 \mathrm{Re}\left[u_1(t)u_2^*(t-\Delta)\right]\mathrm{d}t - 4\int_{-\infty}^{+\infty} |u_2(t-\Delta)|^2 \mathrm{Re}\left[u_2(t-\Delta)u_1^*(t)\right]\mathrm{d}t, \tag{5}$$

where $u_1(t)$ and $u_2(t)$ represent the amplitude functions of solitons. The local minima of the effective potential represent the potential wells for soliton trapping. Because the effective potential arises from the interaction of soliton tails, Eq. 5 is only valid for soliton patterns with separations larger than five times the soliton width.

Data availability

Relevant data supporting the key findings of this study are available within the article and the Supplementary Information file. All raw data generated during the current study are available from the corresponding authors upon request.

Code availability

The code used in this manuscript is available from the corresponding author upon request without any commercial interest.

References

1. Herink, G. et al. Real-time spectral interferometry probes the internal dynamics of femtosecond soliton molecules. *Science* **356**, 50–54 (2017).
2. Jiang, Y., Karpf, S. & Jalali, B. Time-stretch LiDAR as a spectrally scanned time-of-flight ranging camera. *Nat. Photonics* **14**, 14–18 (2019).
3. Krausz, F. & Ivanov, M. Attosecond physics. *Rev. Mod. Phys.* **81**, 163–234 (2009).
4. Witte, S. et al. Deep-ultraviolet quantum interference metrology with ultrashort laser pulses. *Science* **307**, 400–403 (2005).
5. Benedick, A. J., Fujimoto, J. G. & Kärtner, F. X. Optical flywheels with attosecond jitter. *Nat. Photonics* **6**, 97–100 (2012).
6. Jones, D. J. et al. Carrier-envelope phase control of femtosecond mode-locked lasers and direct optical frequency synthesis. *Science* **288**, 635–639 (2000).
7. Riemensberger, J. et al. Massively parallel coherent laser ranging using a soliton microcomb. *Nature* **581**, 164–170 (2020).
8. Zeng, X. et al. Multi-petawatt laser facility fully based on optical parametric chirped-pulse amplification. *Opt. Lett.* **42**, 2014–2017 (2017).
9. Strickland, D. & Morou, G. Chirped pulse amplification. *Opt. Commun.* **56**, 219 (1985).
10. Hentschel, M. et al. Attosecond metrology. *Nature* **414**, 509–513 (2000).
11. Chini, M., Zhao, K. & Chang, Z. The generation, characterization and applications of broadband isolated attosecond pulses. *Nat. Photonics* **8**, 178–186 (2014).
12. Tang, D. Y., Zhao, L. M., Zhao, B. & Liu, A. Q. Mechanism of multisoliton formation and soliton energy quantization in passively mode-locked fiber lasers. *Phys. Rev. A* **72**, 043816 (2005).
13. Cole, D. C. et al. Soliton crystals in Kerr resonators. *Nat. Photonics* **11**, 671–676 (2017).
14. Haboucha, A. et al. Analysis of soliton pattern formation in passively mode-locked fiber lasers. *Phys. Rev. A* **78**, 043806 (2008).
15. Weill, R. et al. Noise-mediated Casimir-like pulse interaction mechanism in lasers. *Optica* **3**, 189–192 (2016).
16. Kutz, J. N., Collings, B. C., Bergman, K. & Knox, W. H. Stabilized pulse spacing in soliton lasers due to gain depletion and recovery. *IEEE J. Quantum Electron* **34**, 1749–1757 (1998).
17. Malomed, B. A. Bound solitons in the nonlinear Schrodinger-Ginzburg-Landau equation. *Phys. Rev. A* **44**, 6954–6957 (1991).
18. Akhmediev, N. N. & Ankiewicz, A. Multisoliton solutions of the complex Ginzburg-Landau equation. *Phys. Rev. Lett.* **79**, 4047 (1997).
19. Wang, Z. Q. et al. Optical soliton molecular complexes in a passively mode-locked fibre laser. *Nat. Commun.* **10**, 830 (2019).
20. Becker, C. et al. Oscillations and interactions of dark and dark–bright solitons in Bose–Einstein condensates. *Nat. Phys.* **4**, 496–501 (2008).
21. Stratmann, M., Pagel, T. & Mitschke, F. Experimental observation of temporal soliton molecules. *Phys. Rev. Lett.* **95**, 143902 (2005).
22. Grelu, P., Belhache, F., Gutty, F. & Soto-Crespo, J. M. Phase-locked soliton pairs in a stretched-pulse fiber laser. *Opt. Lett.* **27**, 966–968 (2002).
23. Krupa, K. et al. Real-time observation of internal motion within ultrafast dissipative optical soliton molecules. *Phys. Rev. Lett.* **118**, 243901 (2017).
24. Zou, D. et al. Synchronization of the internal dynamics of optical soliton molecules. *Optica* **9**, 1307–1313 (2022).

25. Jang, J. K., Erkintalo, M., Coen, S. & Murdoch, S. G. Temporal tweezing of light through the trapping and manipulation of temporal cavity solitons. *Nat. Commun.* **6**, 7370 (2015).
26. Jang, J. K., Erkintalo, M., Murdoch, S. G. & Coen, S. Ultraweak long-range interactions of solitons observed over astronomical distances. *Nat. Photonics* **7**, 657–663 (2013).
27. Wang, Y. et al. Universal mechanism for the binding of temporal cavity solitons. *Optica* **4**, 855–863 (2017).
28. He, W. et al. Synthesis and dissociation of soliton molecules in parallel optical-soliton reactors. *Light.: Sci. Appl.* **10**, 120 (2021).
29. Pang, M., He, W., Jiang, X. & Russell, P. S. J. All-optical bit storage in a fibre laser by optomechanically bound states of solitons. *Nat. Photonics* **10**, 454–458 (2016).
30. He, W. et al. Formation of optical supramolecular structures in a fibre laser by tailoring long-range soliton interactions. *Nat. Commun.* **10**, 5756 (2019).
31. Rotschild, C., Alfassi, B., Cohen, O. & Segev, M. Long-range interactions between optical solitons. *Nat. Phys.* **2**, 769–774 (2006).
32. Nimmesgern, L. et al. Soliton molecules in femtosecond fiber lasers: universal binding mechanism and direct electronic control. *Optica* **8**, 1334–1339 (2021).
33. Kurtz, F., Ropers, C. & Herink, G. Resonant excitation and all-optical switching of femtosecond soliton molecules. *Nat. Photonics* **14**, 9–13 (2019).
34. Liu, S., Cui, Y., Karimi, E. & Malomed, B. A. On-demand harnessing of photonic soliton molecules. *Optica* **9**, 240–250 (2022).
35. Zhu, T. et al. Observation of controllable tightly and loosely bound solitons with an all-fiber saturable absorber. *Photonics Res.* **7**, 61–68 (2018).
36. Girardot, J. et al. On-demand generation of soliton molecules through evolutionary algorithm optimization. *Opt. Lett.* **47**, 134–137 (2022).
37. Luo, C. et al. Real-time comprehensive control over soliton molecules enabled by physics-inspired searching. *Laser Photon. Rev.* **18**, 2401153 (2024).
38. Xu, J. et al. All-in-one, all-optical logic gates using liquid metal plasmon nonlinearity. *Nat. Commun.* **15**, 1726 (2024).
39. Rohrmann, P., Hause, A. & Mitschke, F. Solitons beyond binary: possibility of fibre-optic transmission of two bits per clock period. *Sci. Rep.* **2**, 866 (2012).
40. Vogt, G. et al. Analysis of femtosecond quantum control mechanisms with colored double pulses. *Phys. Rev. A* **74**, 033413 (2006).
41. Takahashi, H. et al. Measurement of group refractive indices of glass using a color-selective multi-pulse generated with a spatial light modulator. *Opt. Lett.* **46**, 1534–1537 (2021).
42. Resan, B., Archundia, L. & Delfyett, P. J. FROG measured high-power 185-fs pulses generated by down-chirping of the dispersion-managed breathing-mode semiconductor mode-locked laser. *IEEE Photonics Technol. Lett.* **17**, 1384–1386 (2005).
43. Nelson, L. E. et al. Ultrashort-pulse fiber ring lasers. *Appl. Phys. B* **65**, 277–294 (1997).
44. Cui, Y. et al. Dichromatic breather molecules in a mode-locked fiber laser. *Phys. Rev. Lett.* **130**, 153801 (2023).
45. Ilday, F. O., Buckley, J. R., Clark, W. G. & Wise, F. W. Self-similar evolution of parabolic pulses in a laser. *Phys. Rev. Lett.* **92**, 213902 (2004).
46. Peng, J. & Zeng, H. Build-up of dissipative optical soliton molecules via diverse soliton interactions. *Laser Photon. Rev.* **12**, 1800009 (2018).
47. Kelly, S. M. J. Characteristic sideband instability of periodically amplified average soliton. *Electron. Lett.* **28**, 806–807 (1992).
48. Diddams, S. A., Vahala, K. & Udem, T. Optical frequency combs: coherently uniting the electromagnetic spectrum. *Science* **369**, eaay3676 (2020).
49. Walmsley, I. A. & Wong, V. Characterization of the electric field of ultrashort optical pulses. *J. Opt. Soc. Am. B* **13**, 2453–2463 (1996).
50. Huang, S. et al. Isomeric dynamics of multi-soliton molecules in passively mode-locked fiber lasers. *APL Photonics* **8**, 036105 (2023).
51. Divitt, S. et al. Ultrafast optical pulse shaping using dielectric metasurfaces. *Science* **364**, 890–894 (2019).
52. Mao, D. et al. Synchronized multi-wavelength soliton fiber laser via intracavity group delay modulation. *Nat. Commun.* **12**, 6712 (2021).
53. Brixner, T., García De Abajo, F. J., Schneider, J. & Pfeiffer, W. Nanoscopic ultrafast space-time-resolved spectroscopy. *Phys. Rev. Lett.* **95**, 093901 (2005).
54. Lukashchuk, A. et al. Dual chirped microcomb based parallel ranging at megapixel-line rates. *Nat. Commun.* **13**, 3280 (2022).
55. Haus, H. A. & Wong, W. S. Solitons in optical communications. *Rev. Mod. Phys.* **68**, 423–444 (1996).
56. Sun, Y. et al. Dynamics of dissipative structures in coherently-driven Kerr cavities with a parabolic potential. *Chaos Solitons Fractals* **176**, 114064 (2023).
57. Zhang, Z.-X. et al. Coherence-controlled chaotic soliton bunch. *Nat. Commun.* **15**, 6148 (2024).
58. Sun, Y. et al. Dissipative Kerr solitons, breathers, and chimera states in coherently driven passive cavities with parabolic potential. *Opt. Lett.* **47**, 6353–6356 (2022).
59. Englebert, N. et al. Bloch oscillations of coherently driven dissipative solitons in a synthetic dimension. *Nat. Phys.* **19**, 1014–1021 (2023).
60. Song, Y. et al. Octave-spanning Kerr soliton frequency combs in dispersion- and dissipation-engineered lithium niobate microresonators. *Light Sci. Appl.* **13**, 225 (2024).
61. Zhang, J. et al. Ultrabroadband integrated electro-optic frequency comb in lithium tantalate. *Nature* **637**, 1096–1103 (2025).
62. Cai, Y. et al. Delayed optical feedback-regulated artificial soliton molecule in a femtosecond optical parametric oscillator. *PhotoniX* **5**, 41 (2024).
63. Lu, Z. et al. Synthesized soliton crystals. *Nat. Commun.* **12**, 3179 (2021).
64. Liu, Y. et al. Phase-tailored assembly and encoding of dissipative soliton molecules. *Light Sci. Appl.* **12**, 123 (2023).
65. Neuenschwander, B. et al. Heat accumulation effects in laser processing of diamond-like nanocomposite films with bursts of femtosecond pulses. *J. Appl. Phys.* **126**, 115301 (2019).
66. Kerse, C. et al. Ablation-cooled material removal with ultrafast bursts of pulses. *Nature* **537**, 84–88 (2016).
67. Yang, W., Kazansky, P. G. & Svirko, Y. P. Non-reciprocal ultrafast laser writing. *Nat. Photonics* **2**, 99–104 (2008).
68. Agrawal, G. P. *Nonlinear Fiber Optics* 3th edn (Academic Press, 2001).

Acknowledgements

This work was supported by the National Key R&D Programme of China (2024YFB4609200 to G.C.), the National Natural Science Foundation of China (12274344 to D.M.) and the Natural Science Basic Research Programme of Shaanxi (2023-JC-YB-563 to C.Z.).

Author contributions

H.Z. and C.Z. performed the experiments, carried out the simulation and wrote the manuscript. D.M. designed the experiment, carried out the theoretical analysis and revised the manuscript. Y.D. and B.J. plotted the figures and discussed the results. G.C., Z.S., X.L., M.P. and J.Z. contributed to the interpretation and revision of the manuscript.

Competing interests

The authors declare no competing interests.

Additional information

Supplementary information The online version contains supplementary material available at https://doi.org/10.1038/s41467-025-59990-x.

Correspondence and requests for materials should be addressed to Dong Mao.

Peer review information *Nature Communications* thanks Stefan Wabnitz who co-reviewed with Yifan Sun; and the other, anonymous, reviewer(s) for their contribution to the peer review of this work. A peer review file is available.